Polymers **2014**, *6*, 2875-2895; doi:10.3390/polym6112875

OPEN ACCESS

polymers

ISSN 2073-4360

www.mdpi.com/journal/polymers

Article

Flame-Retardancy Properties of Intumescent Ammonium Poly(Phosphate) and Mineral Filler Magnesium Hydroxide in Combination with Graphene

Bettina Dittrich [1], Karen-Alessa Wartig [2], Rolf Mülhaupt [2] and Bernhard Schartel [1,*]

[1] BAM Federal Institute for Materials Research and Testing, Unter den Eichen 87, Berlin 12205, Germany; E-Mail: bettina.dittrich@bam.de

[2] Freiburg Materials Research Center and Institute for Macromolecular Chemistry, Albert-Ludwigs-University of Freiburg, Stefan-Meier-Str. 31, Freiburg 79104, Germany; E-Mails: karenalessa.wartig@clariant.com (K.-A.W.); rolf.muelhaupt@makro.uni-freiburg.de (R.M.)

* Author to whom correspondence should be addressed; E-Mail: bernhard.schartel@bam.de; Tel.: +49-30-8104-1021; Fax: +49-30-8104-1747.

External Editor: A. Richard Horrocks

Received: 14 October 2014; in revised form: 11 November 2014 / Accepted: 13 November 2014 / Published: 20 November 2014

Abstract: Thermally reduced graphite oxide (TRGO), containing only four single carbon layers on average, was combined with ammonium polyphosphate (APP) and magnesium hydroxide (MH), respectively, in polypropylene (PP). The nanoparticle's influence on different flame-retarding systems and possible synergisms in pyrolysis, reaction to small flame, fire behavior and mechanical properties were determined. TRGO has a positive effect on the yield stress, which is decreased by both flame-retardants and acts as a synergist with regard to Young's modulus. The applicability and effects of TRGO as an adjuvant in combination with conventional flame-retardants depends strongly on the particular flame-retardancy mechanism. In the intumescent system, even small concentrations of TRGO change the viscosity of the pyrolysing melt crucially. In case of oxygen index (OI) and UL 94 test, the addition of increasing amounts of TRGO to PP/APP had a negative impact on the oxygen index and the UL 94 classification. Nevertheless, systems with only low amounts (≤1 wt%) of TRGO achieved V-0 classification in the UL 94 test and high oxygen indices (>31 vol%). TRGO strengthens the residue structure of MH and therefore functions as a strong synergist in terms of OI and UL 94 classification (from HB to V-0).

Keywords: graphene; intumescence; ammonium polyphosphate; magnesium hydroxide; synergy; polypropylene

1. Introduction

Flame-retardants, like metal hydroxides, intumescent systems or various phosphorous substances, have been extensively investigated and established in many polymers in order to achieve halogen-free and environmentally friendly flame-retardant solutions [1–4]. These systems present various flame-retardancy mechanisms, like gas phase or condensed phase mechanism and physical or chemical actions [5]. High concentrations of halogen-free flame-retardants starting from 20 wt% up to 60 wt% are required to fulfill the parameters and classifications demanded by industry. Especially the very high amounts of metal hydroxides $Al(OH)_3$ and $Mg(OH)_2$ (40 wt% to 60 wt%) often alter the mechanical properties of the composites, rendering them brittle by deteriorating the elongation at break, accompanied by impairing both impact strength and tensile strength [6–9].

Much lower concentrations are required in the case of nanoparticle flame-retardants, like layered silicates, carbon nanotubes, nanometer-sized metal oxides, or polyhedral oligomeric silsesquioxane (POSS) where concentrations of less than 5 wt% to 10 wt% are able to achieve remarkable results to improve the heat release rate and fire behavior of non-charring polymers like polypropylene [10–13]. During combustion of the non-charring polymers, nanoparticles form residue layers on top of the sample, which act as heat shields and reduce the heat input from the gas phase to the pyrolysis zone [14–16]. Nanocomposites burn with the typical features of residue-forming materials and have a peak heat release rate up to 85% lower than the neat polymer [17,18]. Despite their success in the cone calorimeter, nanoparticles are often not efficient in reducing the overall flammability of polymers. The UL 94 classification and oxygen index remain similar or are even worsened by the addition of nanoparticles [19–23]. An increase in nanocomposites' melt viscosity hinders the polymer material from dripping or flowing away from the pyrolysis zone and thus from cooling it. The latest proposals for flame-retardant nanofillers are graphene particles, which have already proved to have the strongest influence on non-charring polymer properties and especially on the burning behavior within the group of carbon (nano)particles [16,19,20].

Nanoparticles were investigated not only as sole polymer fillers, but also as adjuvants and as a replacement for conventional halogen-free flame-retardants, like phosphorous, intumescent or metal hydroxide flame-retardants. To date mainly layered silicates but also carbon nanotubes, POSS, metal oxides and boehmite have been used to enhance the flame retardancy efficiency of halogen-free compounds [24–30]. Thereby, the results for combining conventional flame-retardants varied from worsening the flame retardancy effect to synergistic enhancement. Due to the charring and residue-forming behavior of e.g., intumescent and metal hydroxide flame retardants, but also of charring polymers, the additional nanoparticles do not introduce residue formation as in non-charring polymer systems. Instead, the nanoparticles change the properties of the already existing residue. Their influence ranges from influencing the formation of residue, as in intumescent systems by increased melt viscosity, to mechanical reinforcement and changing the residue surface when combined with metal hydroxides.

The aim of this work is to evaluate the applicability of functionalized graphene (TRGO) prepared by thermal reduction of graphite oxide as an adjuvant in conventional flame-retardants in polypropylene (PP). To this end, two flame retardancy systems were chosen that differ strongly in their modes of action. A commercial intumescent system based on ammonium polyphosphate (APP) was used to represent the physical action of insulation. Intumescent systems build up a cross-linked residue that swells under the release of blowing agents. In the case of intumescent systems, an adjusted melt viscosity in the condensed phase is required in order to guarantee the best possible intumescence. The second conventional flame retardant used was magnesium hydroxide (MH), which works via physical action, combining gas-phase and condensed-phase mechanisms. Upon heating, MH is converted into MgO and H_2O. The strongly endothermic reaction cools the condensed phase, MgO forms a protective layer on top of the sample and H_2O dilutes and cools the gas phase. When combining APP and MH each with graphene, the cooperation between halogen-free flame-retardant and nanoparticle depended strongly on the flame-retardants' modes of action.

2. Experimental Section

2.1. Materials

Impact-modified polypropylene (PP, Moplen EP300K) was supplied by LyondellBasell (Frankfurt, Germany). TRGO (layered morphology, particle surface area of 750 m^2/g measured by the BET (Brunauer–Emmett–Teller) method, equated to stacks of four single graphene layers on average) was produced at the University of Freiburg within the joint research project FUNgraphen. As conventional flame-retardants, two systems with different modes of action were used: An intumescent system based on ammonium polyphosphate (APP) (Budit 3167, Chemische Fabrik Budenheim, Budenheim, Germany) and the mineral filler magnesium hydroxide (MH) (Magnifin H-10, Albemarle, Baton Rouge, LA, USA). The APP concentration of 27.5 wt% used was suggested by the supplier to achieve UL94 V-0 classification. The compositions of the investigated materials are shown in Table 1.

TRGO was synthesized from natural graphite (KFL 99.5, AMG Mining AG, Hauzenberg, Germany) according to the modified Hummers method [31,32], where graphite was oxidized with $KMnO_4$ to yield graphite oxide (GO). After washing and drying, GO was thermally reduced in a rotating tube furnace (Nabertherm, Lilienthal, Germany) equipped with an automated GO feed by rapid heating to 750 °C under inert N_2 atmosphere. The obtained product was thermally reduced graphite oxide (TRGO) in the form of a fluffy black powder, which was used without further purification.

Thermal reduction of GO does not lead to the complete removal of oxygen containing groups on the GO sheets. Compared to the perfect polyaromatic structure of graphene, TRGO yields functional hydroxyl, phenolic and carboxylic groups. In addition, TRGO sheets present a wrinkled architecture due to the formation of structural defects by thermal reduction. The amount of functional groups or in other words the oxygen content of TRGO sheets is controlled by the reduction temperature in the tube furnace. Thereby the oxygen content decreases with increasing furnace temperature. Therefore, TRGO is also referred to as functionalized graphene, which is desirable for further chemical modification, e.g., grafting, of graphene [32,33].

Table 1. Composition of the investigated combinations APP (ammonium polyphosphate) & TRGO (thermally reduced graphite oxide) in PP (polypropylene) and MH (magnesium hydroxide) & TRGO in PP.

Material	ω_{PP} (wt%)	ω_{APP} (wt%)	ω_{MH} (wt%)	ω_{TRGO} (wt%)
PP	100	-	-	-
PP/1TRGO	99	-	-	1
PP/APP	72.5	27.5	-	-
PP/APP/0.5TRGO	72	27.5	-	0.5
PP/APP/1TRGO	71.5	27.5	-	1
PP/APP/2TRGO	70.5	27.5	-	2
PP/53MH	47	-	53	-
PP/53MH/1TRGO	46	-	53	1
PP/59MH	41	-	59	-
PP/59MH/1TRGO	40	-	59	1
PP/60MH	40	-	60	-
PP/60MH/1TRGO	39	-	60	1

To prepare the composites, first TRGO was dispersed in acetone (5 g/L) by applying an ultrasound device Bandelin Sonopuls K76 (Berlin, Germany) [34]. Ground PP powder prepared using a cutting mill M50/80, (Hellweg, Roetgen, Germany) was added to the dispersion. Then acetone was removed under reduced pressure and the TRGO-coated PP powder was dried for one night at 60 °C before compounding.

In a tumbling mixer the flame-retardant systems APP and MH were mixed either with PP powder or with the TRGO-coated PP powder in order to realize the desired compositions. The prepared composite mixtures were melt-extruded using a co-rotating Collin bench-top twin screw compounder (Collin Teach-Line® ZK 25 T, Dr. Collin GmbH, Ebersberg, Germany, L/D = 24 (length to diameter ratio of extruder screw), T_{max} = 210 °C) with an average hold-up time of 1 min and a screw speed of 120 rpm. The extruded granulate was dried overnight and afterwards injection-moulded to test specimens for fire tests on an injection-moulding device K 65/180/55 CX V from Krauss Maffei (Munich, Germany, T_{max} = 210 °C, T_{mould} = 30 °C). Specimens for mechanical stress strain testing were injection-moulded on a Ferromatik Milacron K 40 (Ferromatik Milacron, Malterdingen, Germany, T_{max} = 210 °C, T_{mould} = 30 °C).

2.2. Methods

Thermal decomposition of the polymer composites was investigated via thermogravimetry (TG) on a Netzsch-TG 209 ASC F1 Iris (Netzsch, Selb, Germany). The materials were heated from 30 to 900 °C at a heating rate of 10 °C/min. Samples of the combination APP/TRGO were 10 mg in mass and investigated under air flow of 10 mL/min. Samples of the combination MH/TRGO were 5 mg in mass and investigated under N_2 flow of 10 mL/min. The TG was coupled with a Tensor 27 Fourier-transformed infrared (FTIR) spectrometer (Bruker Optics, Ettlingen, Germany) in order to investigate the gaseous pyrolysis products online. The transfer line and the measuring cell of the FTIR were heated up to 250 °C.

Reaction to a small flame was investigated by measuring the oxygen index (OI) according to ISO 4589 (specimen size 150 mm × 10 mm × 4 mm) using an apparatus by Fire Testing Technology

(FTT, East Grinstead, UK). The UL 94 classification was determined according to IEC 60695-11-10 with a sample size of 125 mm × 13 mm × 3 mm. Investigation of the burning behavior under forced-flaming conditions was carried out on a cone calorimeter by FTT according to ISO 5660. The samples 100 mm × 100 mm × 3 mm in size were irradiated with 50 kW/m^2 and a cone heater-specimen distance of 35 mm. The distance of 35 mm was chosen due to the expected intumescence of samples. The materials were measured only in duplicate when the results showed no deviation above 10% in any characteristic; otherwise three measurements were performed.

The quality of macroscopic residue structure was assessed by visual observation and the microscopic structure inside the residues was investigated by scanning electron microscope (SEM) FEI XL30 ESEM (FEI, Eindhoven, The Netherlands) at 4000× magnification.

Viscosity of the molten intumescent composites was investigated via frequency sweep method (ω = 0.1 to 100 s^{-1}, γ = 0.5%) at 210 °C on a rheometer MCR 501 (Anton Paar, Ostfildern, Germany).

To assess the insulation properties of the residues, the temperature development on the back of the sample was monitored on-line during a cone calorimeter test with 50 kW/m^2. For that reason, a type K thermo element wire (diameter 1 mm) was fastened to the back of the 3-mm-thick cone calorimeter sample (schematic set-up in [35]).

Investigations on mechanical properties were performed using a stress-strain machine (Zwick Z005, Ulm, Germany) compliant with ISO 527-1/2 to obtain the Young's Modulus and yield stress. Notched Charpy impact strength was investigated according to DIN EN ISO 179 under standardized conditions on a Zwick pendulum. The results are the averaged values of ten measurements.

2.3. Quantification of Synergism

Synergism describes the behavior of two additives that cause a greater effect when combined than the sum of the effects of both additives when used alone. Quantification of the synergy in order to improve the synergy discussion was proposed by Weil and Lewin [36] as well as more recently [37,38]. A synergistic behavior of two components affecting a certain material property is assessed by calculating the synergy effect (SE) index according to Equation (1) [39]. For example, Equation (1) is written to assess the co-operation of MH and TRGO in terms of oxygen index (OI). Thereby, *x* and *y* correspond to the weight proportion of both additives. In the case of synergism, the value of SE is greater than 1, a value equals to 1 describes superposition and a value less than 1 describes antagonism.

$$SE_{OI} = \frac{OI_{PP+xMH+yTRGO} - OI_{PP}}{(OI_{PP+xMH} - OI_{PP}) + (OI_{PP+yTRGO} - OI_{PP})} \quad (1)$$

3. Results and Discussion

3.1. Intumescent APP + TRGO

3.1.1. Pyrolysis

In case of intumescent materials burning, stable flames usually do not cover the whole sample surface, so that oxygen is able to reach the pyrolysis zone for thermo-oxidation. Therefore, the TG investigations of PP/APP/TRGO were performed under airflow to simulate a realistic pyrolysis situation in fires.

PP decomposed in two separate steps (Figure 1). The first step between 250 and 400 °C is assigned to the thermal oxidation of PP with charring and formation of 4 wt% residue. Charring of a polymer under oxygen is a complex process that involves oxidation, the formation of double bonds, cyclization and aromatization [40,41]. PP decomposes via the formation and release of CO, CO_2, aldehydes, ketones, carboxylic acids, esters, alkenes, conjugated alkenes and furans [42–44]. The FTIR spectra of the volatile decomposition products of PP at maximum release rate are presented in Figure 2. CO and CO_2 led to their typical set of signals from 600 to 700 cm^{-1} (CO_2), from 2030 to 2225 cm^{-1} (CO) and from 2225 to 2400 cm^{-1} (CO_2). The further detected signals are related to vibrations of C=O stretching in aldehydes, ketones, carboxylic acids and esters (1670 to 1800 cm^{-1}); to C=C stretching in alkenes, conjugated alkenes and furans (1590 to 1670 cm^{-1}, 1510 and 1542 cm^{-1}); to C–H stretching in aldehydes (2700 to 2800 cm^{-1}), in ketones (2937 cm^{-1}), in aliphatic $–CH_3$/$–CH_2–$(2968 cm^{-1}) and in olefinic $=CH_2$ (3078 cm^{-1}); to C–H deformation in olefinic $=CH_2$ (892 cm^{-1}) and aliphatic $–CH_3$/$–CH_2–$ (1460 cm^{-1}); to O–H stretching in carboxylic acids and alcohols (3500 to 3600 cm^{-1}); to C–O stretching in carboxylic acids (1170 cm^{-1}) and to C–C skeletal vibration in aldehydes (1372 cm^{-1}). The second decomposition step of PP led to the total thermal oxidation of the charred residue by releasing CO and CO_2. The decomposition of APP proceeded in two well-known steps [45,46]. Between 290 and 450 °C, condensation and cross-linking of the polyphosphate chains to poly (phosphoric acid) released NH_3 and water. Starting from 450 °C, the cross-linked poly (phosphoric acids) were evaporated or converted into sublimating P_4O_{10} due to further dehydration. The FTIR spectra of the first decomposition step of APP (Figure 2) present typical signals related to N–H stretching and deformation vibrations in NH_3 at 931, 965, 1626 and 3334 cm^{-1}. The mass loss of PP/APP with 27.5 wt% APP presented the same two decomposition steps as APP. Only a very small shoulder from 250 to 300 °C on the mass loss rate curve (Figure 1b) of PP/APP marks the beginning of PP decomposition. After initial release, the volatile oxidation products of PP were trapped in the multiple cells of the swollen residue and released after a delay. After the first decomposition step of PP/APP, a residue of 23 wt% was obtained, corresponding to the expected residue calculated via linear combination of PP and APP mass loss curves. Consequently, no or only slight cross-linking between PP and APP decomposition products is indicated. In addition, APP in PP had no influence on the type of volatile decomposition products, as the FTIR spectra of PP/APP combined the detected signals for PP and APP.

The thermal decomposition of PP/APP/TRGO composites proceeded similar to PP/APP. The addition of increasing TRGO concentrations (0.5 wt%, 1 wt%, 2 wt%) to PP/APP shifted only the end of the first decomposition step, with the release of NH_3, water and PP thermal oxidation products up to 40 °C to higher temperatures. The layered TRGO particles are proposed to strengthen and solidify the structure of the intumescent residue and thereby hinder the diffusion of the volatiles through the residue. The TRGO particles had no influence on the kind of volatiles of PP and APP decomposition, and increased the amount of intumescent residue in proportion to their concentration. This inert behavior has been reported before when TRGO particles were used in PP and halogenated flame-retarded PP [16,19].

Figure 1. (**a**) Mass loss and (**b**) mass loss rate of PP, APP, PP/APP and of the combinations of PP/APP/TRGO under airflow.

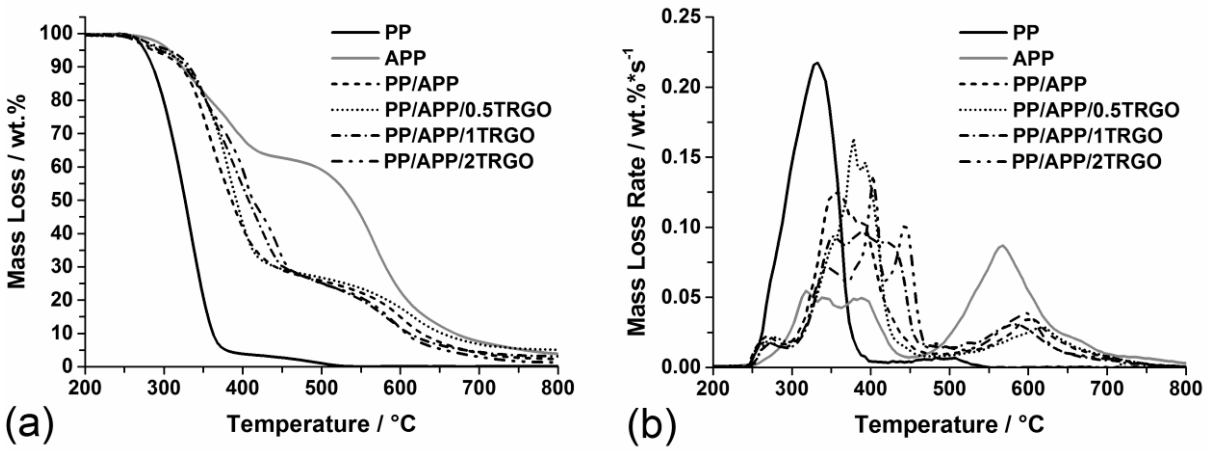

Figure 2. FTIR spectra during maximum mass loss rate of PP decomposition in PP, PP/APP and combinations of PP/APP/TRGO.

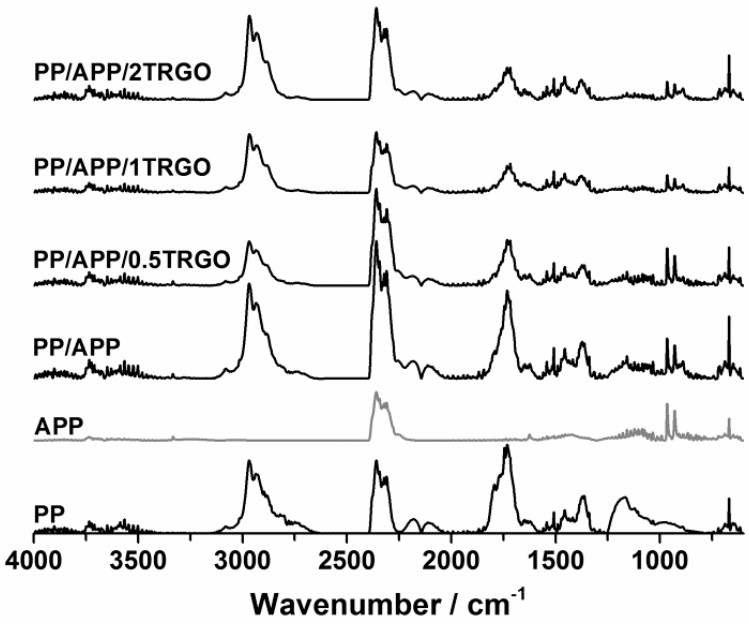

3.1.2. Reaction to Small Flame

27.5 wt% APP in PP led to fast development of an intumescent layer on top of the material. The intumescent layer isolated the pyrolysis zone from the flame heat and reduced the release of combustible pyrolysis gases. Therefore the oxygen index (OI) increased from 19 vol% (PP) to 40 vol% (PP/APP) and the UL 94 classification improved from HB to V-0 (Table 2) thanks to fast extinguishment of the sample bars. With the addition of TRGO to PP/APP, a slower and weaker swelling of the intumescent layer was observed during the OI and UL 94 tests. An increasing nanoparticle content reduced the OI down to 24 vol% in case of 2 wt% TRGO. This result contrasts with the effect of POSS nanoparticles combined with an intumescent flame-retardant system, which caused stronger swelling and an increased OI [26], but is in agreement with results for layered silicate

particles with APP in epoxy resin [47]. Due to the weaker swelling, the time to extinguish the samples in the UL 94 test prolonged with increasing TRGO content. For PP/APP/2TRGO, the samples no longer extinguished and the UL 94 classification changed to HB. Despite the negative impact of TRGO on OI and UL 94 test, PP/APP/0.5TRGO and PP/APP/1TRGO with low TRGO amount presented sufficient intumescence and significantly lower flammability than PP.

Table 2. Reaction to small flame tests for PP, PP/APP and combinations of PP/APP/TRGO.

Material	OI (vol%) Error ± 1	UL 94
PP	19	HB
PP/APP	40	V-0
PP/APP/0.5TRGO	36	V-0
PP/APP/1TRGO	31	V-0
PP/APP/2TRGO	24	HB

3.1.3. Fire Behavior

Intumescent systems show flame retardancy via swelling in the condensed phase to a sponge-like multi-cellular residue that insulates the underlying material from heat transport into the sample. Additionally, the intumescent layer is proposed as a barrier against mass and fuel transport from the condensed phase to the flame zone [4]. In the case of the PP/APP system, the intumescent layer developed immediately and strongly after ignition in the cone calorimeter, forming a first insulating layer on top of the sample. At the beginning of combustion, the heat release rate (HRR) presented a small peak of 100 kW/m^2, but decreased at once with the onset of swelling (Figure 3a), with just a few small flames visible on the edges of the sample. With further swelling in the condensed phase above the aluminum tray (Figure 3b), fuel gases were released from unclosed cells on the edges of residue. This effect increased with increasing residue height and led to a continuously increasing HRR with a PHRR (Peak heat release rate) of 254 kW/m^2, which corresponds to a reduction of 88% compared to PP. At the end of combustion, the intumescent layer of PP/APP was 17 times higher than the original sample thickness (Figure 3b) and formed a fire residue of 14 wt% (Table 3).

Figure 3. (**a**) Heat release rate of PP, PP/APP and combinations of PP/APP/TRGO; intumescent residue after burning of (**b**) PP/APP; (**c**) PP/APP/0.5TRGO; (**d**) PP/APP/1TRGO and (**e**) PP/APP/2TRGO.

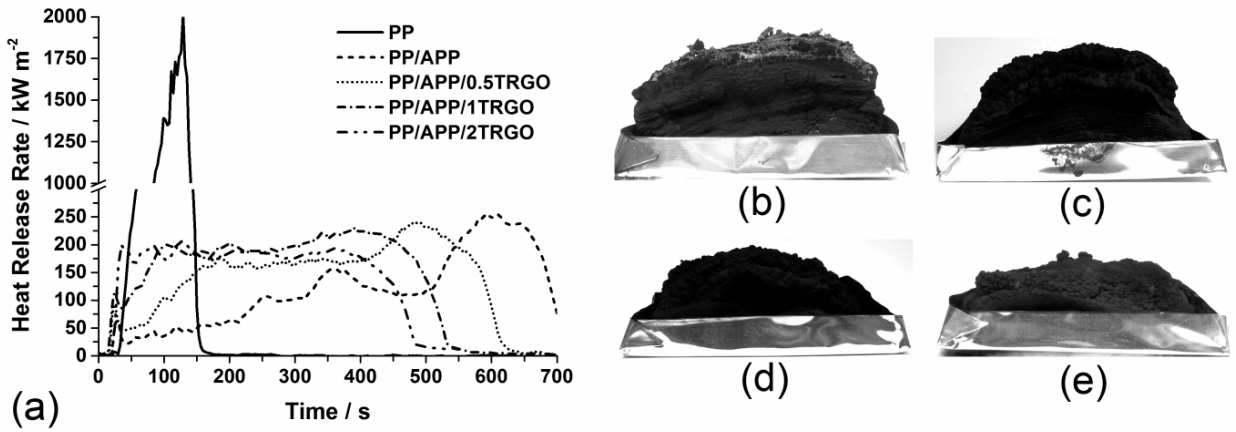

0.5 wt%, 1 wt% and 2 wt% TRGO in PP/APP changed the burning behavior of the composites and their intumescence dramatically. The beginning of the development of intumescence was delayed, with increasing TRGO content and the degree of swelling decreased (Figure 3c–e), similar to layered silicates in combination with APP [47]. The burning behavior changed in the direction of residue-forming materials with the typical shape of HRR curve for PP/APP/2TRGO [18]. The combination of intumescence and residue formation further decreased the PHRR, down to 216 kW/m^2 (89% reduction) in the case of PP/APP/2TRGO. The weaker intumescence of the PP/APP/TRGO composites is caused by increased viscosity in the condensed phase. The viscosity of the condensed phase is a crucial factor for the efficient development of intumescent protection layers [48,49]. When viscosity is too low, the blowing agent NH_3 and H_2O for APP is released easily from the condensed phase via bubbling and no longer available for swelling. In a condensed phase that is too viscous the blowing agent does not generate enough pressure for swelling. Increasing amounts of TRGO increased the melt viscosity of the already optimized commercial intumescent system APP in PP (Figure 4a). The increase in melt viscosity by nanoparticles is a generally known feature and has already been observed for many particles like TRGO, carbon nanotubes and layered silicate [16,19–21]. Nevertheless, the increase in viscosity for low concentrations of 0.5 wt% TRGO appears to be tolerated without altering the swelling behavior of APP. The TRGO particles acted as inert fillers during combustion and increased the residue amount only slightly and in proportion to their concentration (Table 3).

Table 3. Peak heat release rate (PHRR) and residue after combustion of PP, PP/APP and combinations of PP/APP/TRGO.

Material	PHRR (kW/m^2)	Residue (wt%)
PP	2,011 ± 80	0
PP/APP	254 ± 30	14 ± 1
PP/APP/0.5TRGO	243 ± 10	16 ± 1
PP/APP/1TRGO	230 ± 9	16 ± 1
PP/APP/2TRGO	216 ± 9	17 ± 1

Figure 4. (**a**) Melt viscosity at 210 °C over angular frequency of PP, PP/APP and combinations of PP/APP/TRGO and (**b**) temperature development on the back of a cone calorimeter sample during burning under 50 kW/m^2 irradiation.

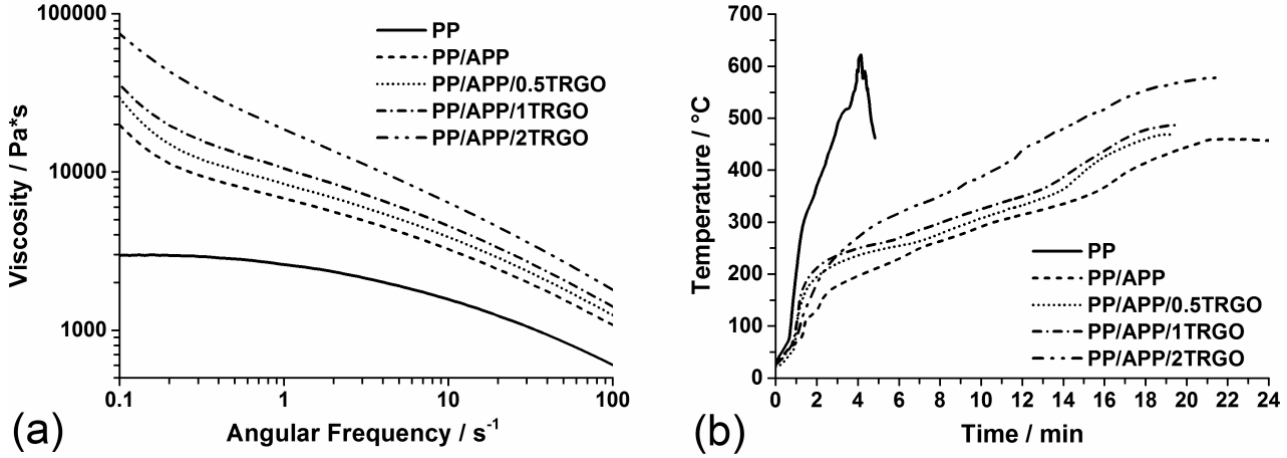

The main commercial application of intumescent systems is the insulation of underlying material from high temperatures in the flame zone and from heat input [49,50]. Figure 4b presents the temperature development on the back of PP, PP/APP and PP/APP/TRGO composite samples during burning in the cone calorimeter and gives information about the insulation efficiency of intumescent layers. At the beginning of irradiation, the heating rates were similar for all investigated materials. As soon as intumescence started to develop, the underlying material was insulated by the foam-like residue. The heating rates decreased and the temperature increase was decelerated in the order of PP < PP/APP/2TRGO < PP/APP/1TRGO < PP/APP/0.5TRGO < PP/APP. Going along with insulation, re-radiation is proposed to occur on the hot residue surface, as was recently described for nanoparticle residues [14,15]. Both factors reduce the effective heat flux penetrating the sample material. After establishing the insulation properties of the swollen residue and the re-radiation, both the effective heat flux and the heating rates became constant. Furthermore, the maximum temperature on the back of the samples decreased and occurred later, with increasing height and faster development of the intumescent layer. In PP/APP the maximum temperature was almost 200 °C lower than the maximum temperature of PP. A direct correlation between insulating properties and the thickness of intumescent layers has also been reported for intumescent coatings on steel plates [51,52].

3.1.4. Mechanical Properties

The mechanical properties Young's modulus, yield strength and Charpy notched impact strength are presented in Table 4. Yield stress decreased by the addition of APP to PP from 26.8 to 20.9 MPa, but increased slightly in the case of PP/TRGO composites, independent of TRGO content. When combined, TRGO was able to counterbalance the negative impact of APP on the yield stress slightly, resulting in an increase from 20.9 to 22.4 MPa compared to PP/APP. The toughness of PP composites represented by the Charpy notched impact strength decreased by the addition of both TRGO and APP filler, both alone and in combination.

Table 4. Mechanical properties: Young's modulus with synergy effect index, yield stress and Charpy notched impact strength of PP/APP/TRGO composites.

Material	Young's modulus (MPa)	Yield stress (MPa)	Charpy notched impact strength (kJ/m²)	$SE_{Young's\ modulus}$
PP	1,270 ± 15	26.8 ± 0.2	9.73 ± 0.95	-
PP/APP	1,840 ± 45	20.9 ± 0.4	2.36 ± 0.15	-
PP/0.5TRGO	1,465 ± 32	27.6 ± 0.3	7.71 ± 0.51	-
PP/1TRGO	1,465 ± 23	27.5 ± 0.1	6.90 ± 0.37	-
PP/2TRGO	1,520 ± 18	27.3 ± 0.3	5.33 ± 0.15	-
PP/APP/0.5TRGO	2,050 ± 20	22.1 ± 0.1	2.64 ± 0.22	1.020
PP/APP/1TRGO	2,080 ± 15	22.1 ± 0.1	2.37 ± 0.04	1.059
PP/APP/2TRGO	2,005 ± 25	22.4 ± 0.2	2.09 ± 0.15	0.896

APP alone and TRGO alone increased the Young's modulus and therefore the stiffness of the resulting composites compared to PP. In PP/APP the Young's modulus was increased by 40% and in PP/TRGO the increase was between 15% and 20% depending on the TRGO content (0.5 wt%,

1 wt% and 2 wt%). The combination of APP with TRGO presented a stronger improvement of stiffness than the single fillers. In PP/APP/0.5TRGO and PP/APP/1TRGO samples, the combination of both additives even resulted in slightly synergistic behavior, with an increase in Young's modulus of 60%. Therefore, the mechanical properties of PP/APP/TRGO composites are characterized by a decrease in toughness accompanied by improved stiffness.

3.2. Mineral Filler $Mg(OH)_2$ + TRGO

3.2.1. Pyrolysis

Under N_2, PP decomposed in one step between 400 and 500 °C, leaving no residue at the end of the test (Figure 5). The mineral filler MH reacted to MgO via the release of 32 wt% water vapor in one step between 300 and 400 °C. The PP/MH composites with 53 wt% and 59 wt% MH presented two slightly overlapping decomposition steps. The first step from 300 to 430 °C is related to the pyrolysis of MH. In case of the PP/MH composites, the end of MH decomposition and its maximum mass loss rate (MLR) shifts to higher temperatures as the gaseous water has to diffuse through the polymer melt before release. As the polymer is filled with particles, increased melt viscosity is presumed, as already shown by Hornsby for another PP/magnesium hydroxide system [53], resulting in slow diffusion. Complete pyrolysis of PP from PP/MH composites took place between approximately 400 and 500 °C, similar to PP alone. Several polymer/$Mg(OH)_2$ systems have already been tested where the addition of the filler had no significant influence on the decomposition behavior of the polymer [54–56]. A strongly reduced MLR in step two originated from the replacement of matrix polymer PP by a large amount of MH filler. After the end of PP pyrolysis, the residue remaining amounts to 35 wt% from PP/53MH and 39 wt% from PP/59MH, respectively, which correspond to the theoretical yield of MgO within the measurement uncertainty.

Figure 5. (**a**) Mass loss and (**b**) mass loss rate of PP, MH, PP/MH and of the combinations of PP/MH/TRGO under N_2 flow.

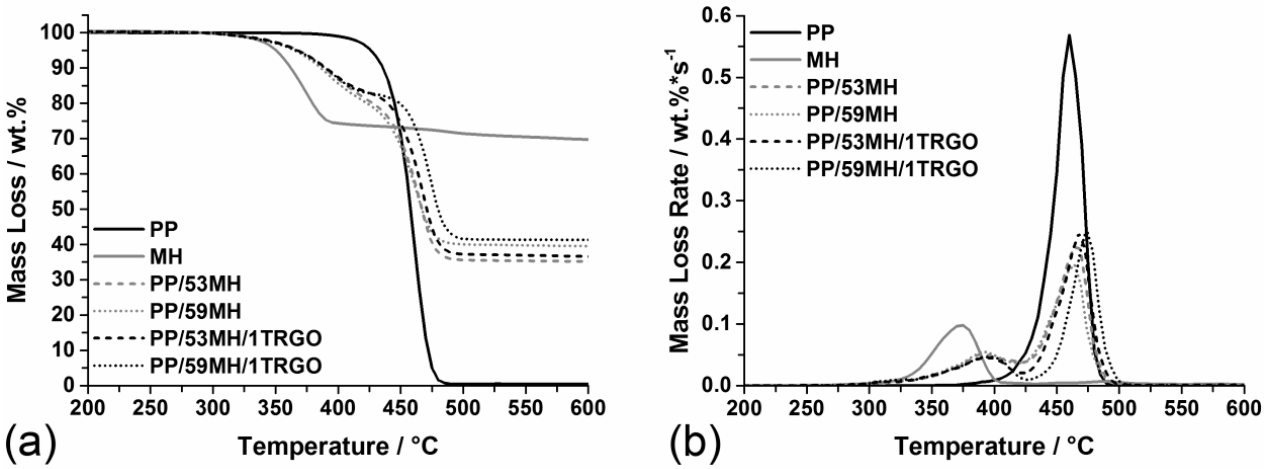

The addition of 1 wt% TRGO to PP/53MH and PP/59MH had no influence on the decomposition behavior of MH, but shifted the pyrolysis of the matrix polymer PP to higher temperatures. Due to a supposed further increase in melt viscosity by TRGO in PP/MH, the diffusion of PP pyrolysis gases

through the polymer melt and their release are decelerated. A shift in pyrolysis temperatures to higher temperatures and therefore stabilization of the polymer was also observed for the combination of $Al(OH)_3$ with layered silicates in ethylene-vinyl acetate [57]. With increasing MH content, the shift in pyrolysis temperatures was more pronounced. The combination of 53 wt% MH with TRGO presented an influence only on the T_{onset}. As PP decomposition proceeds, less polymer melt is available to hold back the pyrolysis gases. The residue consisting of MgO and TRGO was not effective in hindering the diffusion of the gaseous pyrolysis products. The effect of a shift in only T_{onset} is also known for TRGO and other carbon particles like carbon black and carbon nanotubes [16,19,20]. The combination of 59 wt% MH with TRGO shifted the entire decomposition step to higher temperatures. The particle residue structure of PP/59MH/1TRGO is proposed to be closely packed, hindering the diffusion of gases through the residue even without a polymer matrix. At the end of thermal decomposition, the addition of 1 wt% TRGO to PP/53MH and to PP/59MH increased the residue amount slightly in correspondence to the very small amount of TRGO used.

Under inert atmosphere, the decomposition of PP proceeds via radical chain scission, releasing aliphatic and olefinic compounds with the structural groups $–CH_3$, $–CH_2–$ and $=CH_2$ [58,59]. Stretching and bending vibrations of C–C double and single bonds and of C-H bonds produced signals in the FTIR spectra (Figure 6) at 2960 cm^{-1}, 2875 cm^{-1}, 2733 cm^{-1}, 1460 cm^{-1}, 1379 cm^{-1}, 1150 cm^{-1}, 969 cm^{-1}, 806 cm^{-1} (related to $–CH_3$ group), 2920 cm^{-1}, 2850 cm^{-1} (related to $–CH_2–$ group), 3079 cm^{-1}, 1785 cm^{-1}, 1645 cm^{-1} and 887 cm^{-1} (related to $=CH_2$ group). The detected FTIR signals of pyrolysis gases are the same for PP/MH and PP/MH/1TRGO as for PP. As there is also no additional charring of the polymer, it is proposed that MH and MH/TRGO do not react with the pyrolysis products of PP and have no interactions. MH and TRGO appear as inert fillers under anaerobic pyrolysis conditions.

Figure 6. FTIR spectra during maximum mass loss rate of PP decomposition in PP, PP/MH and combinations of PP/MH/TRGO.

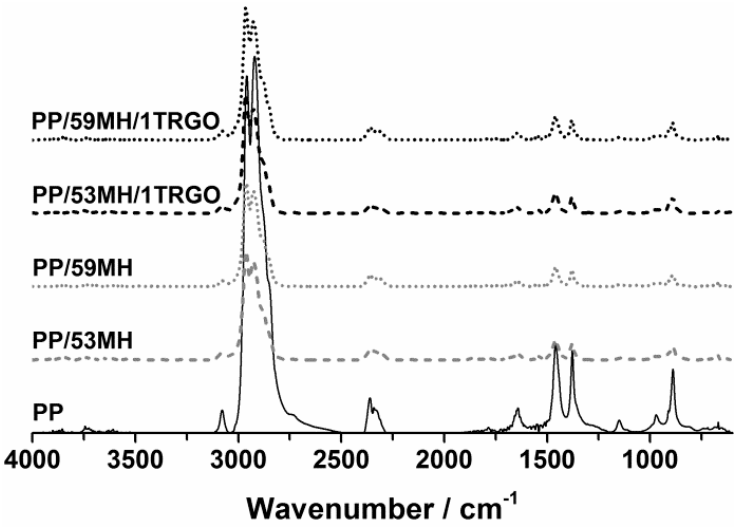

3.2.2. Reaction to Small Flame

The addition of MH in the range of concentrations from 53 wt% to 60 wt% to PP increased the oxygen index (OI) from 19 vol% (PP) up to 32 vol% (PP/59MH) (Table 5). With increasing MH content, a higher oxygen concentration is required to sustain candle-like burning of the sample, as the fuel in the gas phase is more and more diluted by the release of water vapour from MH. Additionally, increased formation of MgO residue on top of the sample is proposed to improve the heat shielding of the OI samples, to decelerate pyrolysis and to act as barriers against the release of pyrolysis gases. Therefore MH reduces the fuel supply in the gas phase. In the UL 94 test, composites with 53 wt% MH and 59 wt% MH were HB classified, similar to PP. Only for PP/60MH did effective flame retardancy of MH take place, enabling the sample to extinguish within 30 s without dripping and to improve the UL 94 classification from HB to V-1.

Table 5. Reaction to small flame tests for PP, PP/MH and combinations of PP/MH/TRGO.

Material	OI (vol%) Error ± 1	SE_{OI}	UL 94
PP	19	-	HB
PP/1TRGO	19	-	HB
PP/53MH	28	-	HB
PP/59MH	32	-	HB
PP/60MH	31	-	V-1
PP/53MH/1TRGO	30	1.341	V-0
PP/59MH/1TRGO	38	1.445	V-0
PP/60MH/1TRGO	35	1.276	V-0

Combining the different PP/MH composites with 1 wt% TRGO increased the OI further by 3 vol% to 5 vol%, with the highest OI observed for PP/59MH/1TRGO (37 vol%). TRGO alone in PP/1TRGO had no influence on the OI. But in combination with MH, TRGO increased the OI, which indicates synergism between both fillers. The synergistic behavior is supported by SE_{OI} values between 1.276 and 1.445, which were achieved for all PP/MH/TRGO combinations. In the UL 94 test, an improvement from HB/V-1 to V-0 was observed for all investigated MH concentrations when combined with 1 wt% TRGO. As PP/1TRGO was HB-classified, MH and TRGO show synergism in terms of UL 94 classification as well. TRGO is supposed to improve the residue structure of MgO, which leads to easier extinguishment of the sample by increasing the efficiency of heat shielding and through an improved barrier against fuel release.

3.2.3. Fire Behavior

In the cone calorimeter, PP burnt with the typical features of a non-residue-forming material with a peak heat release rate (PHRR) of 2011 kW/m^2 (Figure 7a, Table 6) [18]. 53 wt% to 60 wt% MH reduced the PHRR of PP/MH composites by 88% to 89% compared to PP via the combination of several flame retardancy mechanisms [5,60,61]. Due to the high concentration of MH in the composites, the matrix polymer PP is strongly diluted and much less material is available for combustion. Water vapor released during thermal decomposition of MH cools the gas phase and dilutes the fuel, so that the effective heat of combustion (THE (total heat evolved)/TML (total mass loss), Table 6)

decreased with increasing MH content from 4.1 (PP) to 2.9 MJ/m^2·g (PP/60MH). The heating of the condensed phase is decelerated by the endothermic decomposition reaction of MH and by the heat-shielding effect of the MgO residue on top of the sample. Heat-shielding effects are reported for nanoparticles whose flame retardancy mechanism is based on residue formation [14–16,35]. Therefore, MH changed the burning behavior of PP/MH composites strongly in the direction of typical residue-forming materials. Typical features include prolonged burning time, a constant heat release rate (HRR) during combustion, a reduced PHRR and the shift of the PHRR to the beginning of combustion. Figure 7b shows the temperature development on the back of PP and PP/60MH cone calorimeter samples during burning to give insight into the shielding effect in PP/MH composites. Directly after ignition, MgO residue formation has not yet taken place and the heating rates of PP and PP/60MH are similar. Due to the similar heating rates, heat release increased at the same rate in PP and in PP/MH composites. With proceeding combustion, MgO residue formed by migration and agglomeration of the particles and the effective heat flux from flame and external heat source is reduced by re-radiation on the residue surface. Therefore the heating rates of PP/MH composites started to decrease. Heating of the pyrolysis zone and pyrolysis itself was retarded, leading to reduced fuel release rates and therefore to a declining HRR. As soon as the effective heat flux into the sample is stabilized by the formation of residue, the heating rate of the sample and the HRR becomes constant. The PHRR of PP/MH composites decreased with increasing MH content (Table 6).

The heat-shielding efficiency of a residue is determined by the macroscopic and microscopic residue structure, as already shown for CB (carbon black) and TRGO in PP and for the combination of layered silicates with low-melting silicate glass in epoxy resin [16,62]. The residue structures of PP/MH composites improved with increasing MH content (Figure 8a,c). 53 wt% MH formed a residue that covers the entire macroscopic surface but consists of loosely arranged agglomerates without cohesion. The residue of 59 wt% presented a more uniform surface with larger agglomerated units. The microscopic structure of the PP/59MH residue also appeared denser and more stable than the PP/53MH residue.

Figure 7. (**a**) Heat release rate of PP, PP/MH and combinations of PP/MH/TRGO and (**b**) temperature development on the back of PP, PP/60MH and PP/60MH/1TRGO cone calorimeter samples during burning at 50 kW/m^2 irradiation.

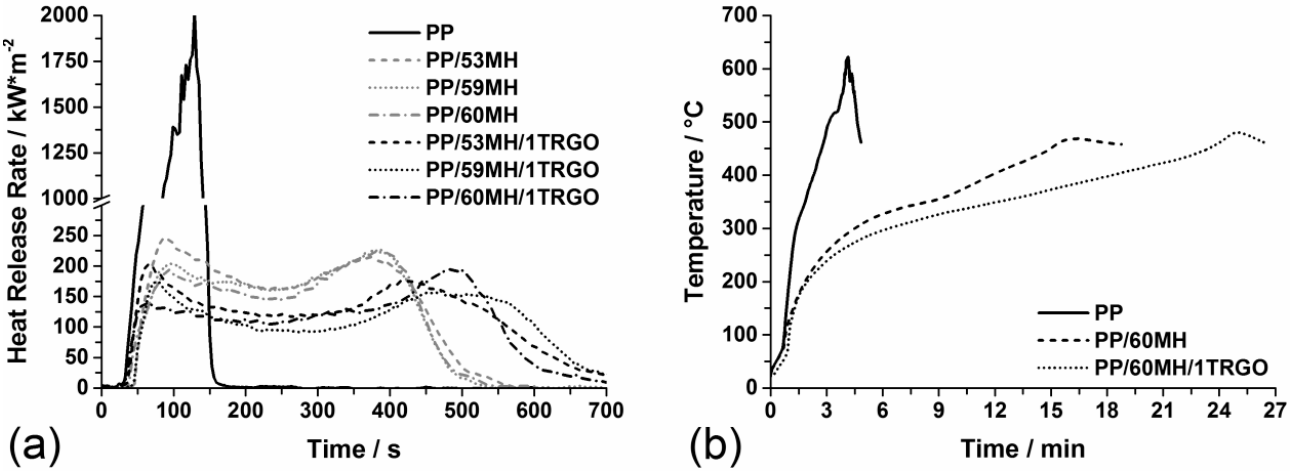

Table 6. Peak heat release rate (PHRR), total heat evolved (THE), residue and effective heat of combustion (THE/TML (total mass loss)) of PP, PP/MH and combinations of PP/MH/TRGO.

Material	PHRR (kW/m^2)	THE (MJ/m^2)	Residue (wt%)	THE/TML (MJ/m^2·g)
PP	2,011 ± 80	106 ± 4	0	4.1 ± 0.2
PP/53MH	240 ± 10	81 ± 3	33 ± 1	3.2 ± 0.1
PP/59MH	226 ± 9	75 ± 3	38 ± 2	3.0 ± 0.1
PP/60MH	225 ± 9	72 ± 3	40 ± 2	2.9 ± 0.1
PP/53MH/1G	203 ± 8	82 ± 3	34 ± 1	3.2 ± 0.1
PP/59MH/1G	181 ± 7	75 ± 3	38 ± 2	3.0 ± 0.1
PP/60MH/1G	190 ± 8	72 ± 3	41 ± 2	3.0 ± 0.1

Figure 8. Macroscopic surface structure and microscopic structure of cone calorimeter residues of (**a**) PP/53MH; (**b**) PP/53MH/1TRGO; (**c**) PP/59MH and (**d**) PP/59MH/1TRGO.

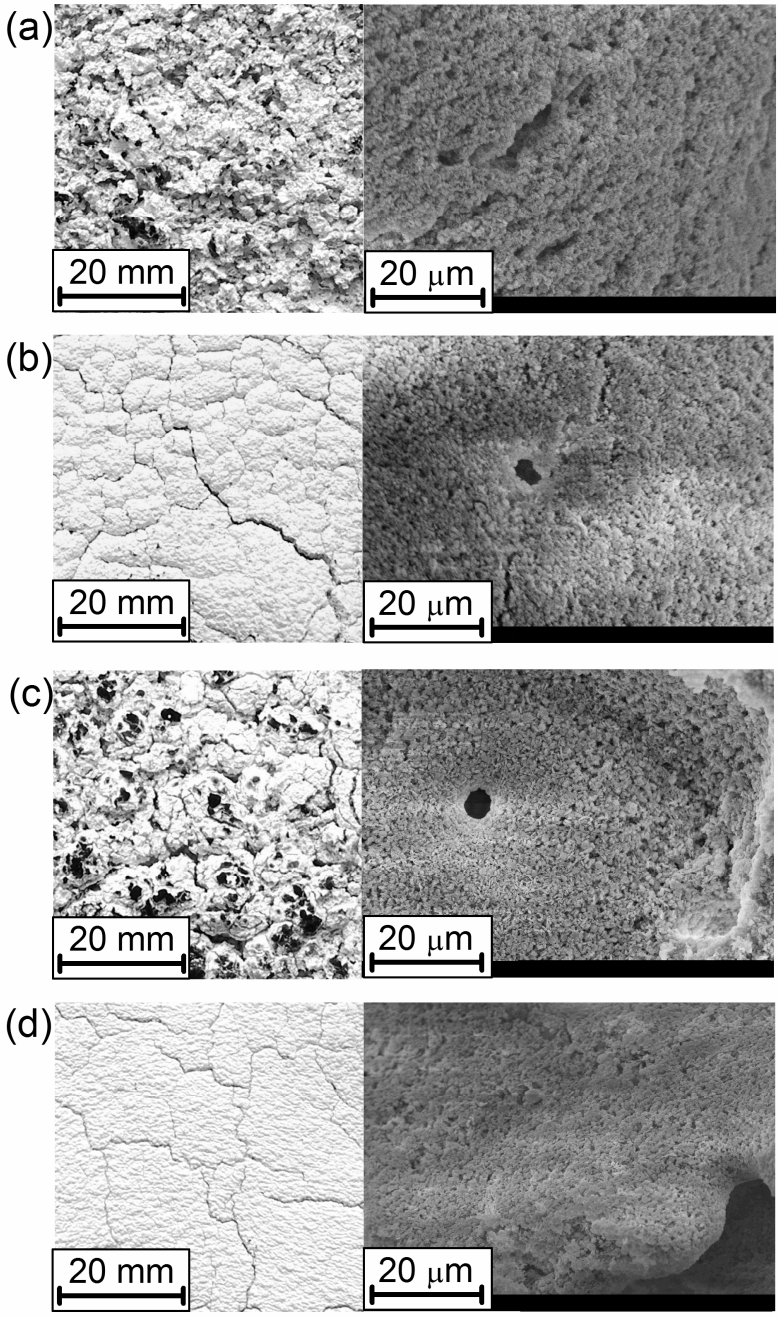

Addition of 1 wt% TRGO to the PP/MH composites further reduced the HRR during combustion so that the PHRR occurred directly after ignition and before the formation of protective residue layers (Figure 7a). Compared to PP, the combination of MH with TRGO reduced the PHRR (peak heat release rate) by up to 91% from 2011 to 181 kW/m^2. TRGO improved the heat-shielding efficiency of the obtained residue, leading to further reduced heating rates of the underlying material once the residue formed on top of the sample (Figure 7b). The residues of PP/53MH/1TRGO and PP/59MH/1TRGO in Figure 8b,d presented a superior structure to the residues of PP/MH composites. The residues had a smooth, uniform surface structure and appeared to be stable and flexible at the same time. Despite moving and deforming of the sample during the test, the residue did not tear open. The microscopic structure was also improved by adding TRGO to the PP/MH composites. TRGO particles are proposed to fill the gaps between the MgO particles and are proposed to densify the residue agglomerates. During combustion, TRGO particles acted as inert fillers, presenting only condensed-phase mechanisms and exerting no influence on the effective heat of combustion of the PP/MH/TRGO composites (Table 6). Due to their inert character and small amount of 1 wt%, TRGO particles did not significantly change the THE (total heat evolved) or the amount of residue.

3.2.4. Mechanical Properties

The influence of MH and MH in combination with TRGO on the mechanical properties of PP composites is listed in Table 7. MH alone in PP reduced the yield stress of PP, whereas additional TRGO is able to counteract the reduction slightly through its positive effect on yield stress. Nevertheless, all composites had a low yield stress compared to neat PP. An enormous increase in flexibility was observed by the addition of MH to PP, probably due to the fatty-acid coating of MH particles. The Charpy notched impact strength increased from 9.7 kJ/m^2 for PP up to 35.6 kJ/m^2 in the case of PP/54MH. TRGO, in contrast, decreased the impact strength of PP/1TRGO and also had a negative effect on toughness when used in in combination with MH in PP composites. Nevertheless, the impact strength of PP/MH/1TRGO is still 50% higher than the impact strength of PP. By adding MH to neat PP an immense improvement of stiffness occurred with an augmentation of Young's modulus of up to 150% compared to PP with increasing MH concentration. Combining MH with 1 wt% TRGO in PP/MH/1TRGO systems increased the Young's modulus even further and more strongly than the sum of the single fillers. TRGO and MH presented synergistic behavior in all combinations investigated.

Table 7. Mechanical properties: Young's modulus with synergy effect index, yield stress and Charpy notched impact strength of PP/MH/TRGO composites.

Material	Young's modulus (MPa)	Yield stress (MPa)	Charpy notched impact strength (kJ/m²)	$SE_{Young's\ modulus}$
PP	1,270 ± 15	26.8 ± 0.2	9.73 ± 0.95	-
PP/1TRGO	1,465 ± 23	27.5 ± 0.1	6.90 ± 0.37	-
PP/53MH	2,950 ± 70	16.3 ± 0.2	29.0 ± 3.10	-
PP/54MH	2,990 ± 25	15.7 ± 0.0	35.6 ± 2.62	-
PP/59MH	3,140 ± 15	15.7 ± 0.2	29.0 ± 2.46	-
PP/53MH/1G	3,150 ± 30	16.9 ±0.1	14.1 ± 0.92	1.003
PP/54MH/1G	3,400 ± 25	16.9 ± 0.1	13.8 ± 0.95	1.113
PP/59MH/1G	3,500 ± 20	16.8 ± 0.0	13.4 ± 0.99	1.080

4. Conclusions

The applicability of TRGO as a flame retardancy adjuvant for a commercial intumescent ammonium polyphosphate (APP) system and for the mineral filler magnesium hydroxide (MH) was investigated. The cooperation between TRGO and conventional flame retardant depended strongly on the modes of action. In combination with APP, TRGO influenced mainly the development of intumescence due to the increase in condensed-phase viscosity with increasing TRGO content. Swelling was decelerated, the height of the resulting protective layer decreased and the burning behavior changed to residue-forming materials with increasing TRGO content. Decreasing height of swelling resulted in decreased insulation properties of the intumescent layer against heat input from the flame. With very low concentrations of TRGO up to 1 wt%, the effect of the viscosity increase did not yet influence the reaction to small flame of PP/APP/TRGO composites, so that a high oxygen index and UL 94 V-0 classification were achieved, similar to PP/APP. But with increasing TRGO content of >1 wt%, a decrease in OI and worsening of the UL 94 classification from V-0 to HB occurred. To achieve the best possible intumescence for PP/APP/TRGO, the combination with plasticisers is proposed to adjust the ideal condensed-phase viscosity. In combination with MH, TRGO densified the particle network in the composites and increased thermal stability against pyrolysis by shifting the T_{onset} and T_{max} of PP decomposition in PP/MH/TRGO composites to higher temperatures. During combustion, TRGO strongly enhanced the surface structure and the microscopic structure of the MH residue. The resulting effective heat shielding led to an improvement, especially in the reaction to small flame. MH and TRGO acted synergistically and improved the UL 94 classification from HB/V-1 for PP/MH to V-0 for PP/MH/TRGO and increased the oxygen index strongly with addition of TRGO to PP/MH. Due to the synergy, the overall amount of flame retardant additives required decreases for the combination of MH with TRGO. In the cone calorimeter, improved heat shielding in PP/MH/TRGO presented better insulation properties than PP/MH and further decreased the heat release rate. TRGO presented positive effects on the yield stress and even synergistic effects on the Young's modulus of the composites in both the intumescent system and the MH system.

Acknowledgments

The authors would like to thank Volker Altstädt and TuTech Innovation GmbH in Hamburg for help in specimen preparation. They are also grateful for rheology measurements performed by Christian Huth at BAM. This study is part of the FUNgraphen project funded by BMBF (03X0111C).

Conflicts of Interest

The authors declare no conflict of interest.

References

1. Schartel, B. Phosphorus-based flame retardancy mechanisms—Old hat or a starting point for future development? *Materials* **2010**, *3*, 4710–4745.
2. Levchik, S.V.; Weil, E.D. A review of recent progress in phosphorus-based flame retardants. *J. Fire Sci.* **2006**, *24*, 345–364.

3. Weil, E.A.; Levchik, S.V. Flame retardants in commercial use or development for polyolefins. *J. Fire Sci.* **2008**, *26*, 5–43.
4. Bourbigot, S.; Le Bras, M.; Duquesne, S.; Rochery, M. Recent advances for intumescent polymers. *Macromol. Mater. Eng.* **2004**, *289*, 499–511.
5. Levchik, S.V. Introduction to flame retardancy and polymer flammability. In *Flame Retardant Polymer Nanocomposites*; John Wiley & Sons, Inc.: Hoboken, NJ, USA, 2006; pp. 1–29.
6. Camino, G.; Maffezzoli, A.; Braglia, M.; de Lazzaro, M.; Zammarano, M. Effect of hydroxides and hydroxycarbonate structure on fire retardant effectiveness and mechanical properties in ethylene-vinyl acetate copolymer. *Polym. Degrad. Stab.* **2001**, *74*, 457–464.
7. Hornsby, P.R.; Watson, C.L. Interfacial modification of polypropylene composites filled with magnesium hydroxide. *J. Mater. Sci.* **1995**, *30*, 5347–5355.
8. Zhang, X.; Guo, F.; Chen, J.; Wang, G.; Liu, H. Investigation of interfacial modification for flame retardant ethylene vinyl acetate copolymer/alumina trihydrate nanocomposites. *Polym. Degrad. Stab.* **2005**, *87*, 411–418.
9. Hippi, U.; Mattila, J.; Korhonen, M.; Seppälä, J. Compatibilization of polyethylene/aluminum hydroxide (PE/ATH) and polyethylene/magnesium hydroxide (PE/MH) composites with functionalized polyethylenes. *Polymer* **2003**, *44*, 1193–1201.
10. Gilman, J.W. Flammability and thermal stability studies of polymer layered-silicate (clay) nanocomposites. *Appl. Clay Sci.* **1999**, *15*, 31–49.
11. Kashiwagi, T.; Grulke, E.; Hilding, J.; Harris, R.; Awad, W.; Douglas, J. Thermal degradation and flammability properties of poly(propylene)/carbon nanotube composites. *Macromol. Rapid Commun.* **2002**, *23*, 761–765.
12. Gallo, E.; Braun, U.; Schartel, B.; Russo, P.; Acierno, D. Halogen-free flame retarded poly(butylene terephthalate) (PBT) using metal oxides/PBT nanocomposites in combination with aluminium phosphinate. *Polym. Degrad. Stab.* **2009**, *94*, 1245–1253.
13. Fina, A.; Abbenhuis, H.C.L.; Tabuani, D.; Camino, G. Metal functionalized poss as fire retardants in polypropylene. *Polym. Degrad. Stab.* **2006**, *91*, 2275–2281.
14. Schartel, B.; Weiss, A. Temperature inside burning polymer specimens: Pyrolysis zone and shielding. *Fire Mater.* **2010**, *34*, 217–235.
15. Wu, G.M.; Schartel, B.; Bahr, H.; Kleemeier, M.; Yu, D.; Hartwig, A. Experimental and quantitative assessment of flame retardancy by the shielding effect in layered silicate epoxy nanocomposites. *Combust. Flame* **2012**, *159*, 3616–3623.
16. Dittrich, B.; Wartig, K.A.; Hofmann, D.; Mülhaupt, R.; Schartel, B. Flame retardancy through carbon nanomaterials: Carbon black, multiwall nanotubes, expanded graphite, multi-layer graphene and graphene in polypropylene. *Polym. Degrad. Stab.* **2013**, *98*, 1495–1505.
17. Kashiwagi, T.; Grulke, E.; Hilding, J.; Groth, K.; Harris, R.; Butler, K.; Shields, J.; Kharchenko, S.; Douglas, J. Thermal and flammability properties of polypropylene/carbon nanotube nanocomposites. *Polymer* **2004**, *45*, 4227–4239.
18. Schartel, B.; Hull, T.R. Development of fire-retarded materials—Interpretation of cone calorimeter data. *Fire Mater.* **2007**, *31*, 327–354.

19. Dittrich, B.; Wartig, K.A.; Hofmann, D.; Mülhaupt, R.; Schartel, B. Carbon black, multiwall carbon nanotubes, expanded graphite and functionalized graphene flame retarded polypropylene nanocomposites. *Polym. Adv. Technol.* **2013**, *24*, 916–926.
20. Dittrich, B.; Wartig, K.A.; Hofmann, D.; Mülhaupt, R.; Schartel, B. The influence of layered, spherical, and tubular carbon nanomaterials' concentration on the flame retardancy of polypropylene. *Polym. Compos.* **2014**, doi:10.1002/pc.23027.
21. Bartholmai, M.; Schartel, B. Layered silicate polymer nanocomposites: New approach or illusion for fire retardancy? Investigations of the potentials and the tasks using a model system. *Polym. Adv. Technol.* **2004**, *15*, 355–364.
22. Schartel, B.; Pötschke, P.; Knoll, U.; Abdel-Goad, M. Fire behaviour of polyamide 6/multiwall carbon nanotube nanocomposites. *Eur. Polym. J.* **2005**, *41*, 1061–1070.
23. Schartel, B.; Braun, U.; Knoll, U.; Bartholmai, M.; Goering, H.; Neubert, D.; Potschke, P. Mechanical, thermal, and fire behavior of bisphenol a polycarbonate/multiwall carbon nanotube nanocomposites. *Polym. Eng. Sci.* **2008**, *48*, 149–158.
24. Bourbigot, S.; Bras, M.L.; Dabrowski, F.; Gilman, J.W.; Kashiwagi, T. PA-6 clay nanocomposite hybrid as char forming agent in intumescent formulations. *Fire Mater.* **2000**, *24*, 201–208.
25. Pawlowski, K.H.; Schartel, B. Flame retardancy mechanisms of aryl phosphates in combination with boehmite in bisphenol a polycarbonate/acrylonitrile-butadiene-styrene blends. *Polym. Degrad. Stab.* **2008**, *93*, 657–667.
26. Vannier, A.; Duquesne, S.; Bourbigot, S.; Castrovinci, A.; Camino, G.; Delobel, R. The use of POSS as synergist in intumescent recycled poly(ethylene terephthalate). *Polym. Degrad. Stab.* **2008**, *93*, 818–826.
27. Beyer, G. Flame retardancy of nanocomposites based on organoclays and carbon nanotubes with aluminium trihydrate. *Polym. Adv. Technol.* **2006**, *17*, 218–225.
28. Schartel, B.; Knoll, U.; Hartwig, A.; Pütz, D. Phosphonium-modified layered silicate epoxy resins nanocomposites and their combinations with ATH and organo-phosphorus fire retardants. *Polym. Adv. Technol.* **2006**, *17*, 281–293.
29. Gallo, E.; Schartel, B.; Acierno, D.; Russo, P. Flame retardant biocomposites: Synergism between phosphinate and nanometric metal oxides. *Eur. Polym. J.* **2011**, *47*, 1390–1401.
30. Lu, H.D.; Wilkie, C.A. Study on intumescent flame retarded polystyrene composites with improved flame retardancy. *Polym. Degrad. Stab.* **2010**, *95*, 2388–2395.
31. Hummers, W.S.; Offeman, R.E. Preparation of graphitic oxide. *J. Am. Chem. Soc.* **1958**, *80*, 1339.
32. Tölle, F.J.; Fabritius, M.; Mülhaupt, R. Emulsifier-free graphene dispersions with high graphene content for printed electronics and freestanding graphene films. *Adv. Funct. Mater.* **2012**, *22*, 1136–1144.
33. Steurer, P.; Wissert, R.; Thomann, R.; Mülhaupt, R. Functionalized graphenes and thermoplastic nanocomposites based upon expanded graphite oxide. *Macromol. Rapid Commun.* **2009**, *30*, 316–327.
34. Kalaitzidou, K.; Fukushima, H.; Drzal, L.T. A new compounding method for exfoliated graphite-polypropylene nanocomposites with enhanced flexural properties and lower percolation threshold. *Compos. Sci. Technol.* **2007**, *67*, 2045–2051.
35. Fina, A.; Cuttica, F.; Camino, G. Ignition of polypropylene/montmorillonite nanocomposites. *Polym. Degrad. Stab.* **2012**, *97*, 2619–2626.

36. Weil, E.D. Synergists, adjuvants and antagonists in flame-retardant systems. In *Fire Retardancy of Polymeric Materials*; CRC Press: Boca Raton, FL, USA, 2000; pp. 115–145.
37. Despinasse, M.C.; Schartel, B. Aryl phosphate–aryl phosphate synergy in flame-retarded bisphenol a polycarbonate/acrylonitrile-butadiene-styrene. *Thermochim. Acta* **2013**, *563*, 51–61.
38. Horrocks, A.R.; Smart, G.; Nazaré, S.; Kandola, B.; Price, D. Quantification of zinc hydroxystannate and stannate synergies in halogen-containing flame-retardant polymeric formulations. *J. Fire Sci.* **2009**, doi:10.1177/0734904109344302.
39. Wu, G.M.; Schartel, B.; Yu, D.; Kleemeier, M.; Hartwig, A. Synergistic fire retardancy in layered-silicate nanocomposite combined with low-melting phenysiloxane glass. *J. Fire Sci.* **2012**, *30*, 69–87.
40. Zanetti, M.; Bracco, P.; Costa, L. Thermal degradation behaviour of PE/clay nanocomposites. *Polym. Degrad. Stab.* **2004**, *85*, 657–665.
41. Levchik, S.; Wilkie, C.A. Char formation. In *Fire Retardancy of Polymeric Materials*; CRC Press: Boca Raton, FL, USA, 2000; pp. 171–215.
42. Adams, J.H. Analysis of the nonvolatile oxidation products of polypropylene I. Thermal oxidation. *J. Polym. Sci. A Polym. Chem.* **1970**, *8*, 1077–1090.
43. François-Heude, A.; Richaud, E.; Leprovost, J.; Heninger, M.; Mestdagh, H.; Desnoux, E.; Colin, X. Real-time quantitative analysis of volatile products generated during solid-state polypropylene thermal oxidation. *Polym. Test.* **2013**, *32*, 907–917.
44. Hoff, A.; Jacobsson, S. Thermal oxidation of polypropylene in the temperature range of 120–280 °C. *J. Appl. Polym. Sci.* **1984**, *29*, 465–480.
45. Camino, G.; Costa, L.; Trossarelli, L. Study of the mechanism of intumescence in fire retardant polymers: Part I—Thermal degradation of ammonium polyphosphate-pentaerythritol mixtures. *Polym. Degrad. Stab.* **1984**, *6*, 243–252.
46. Duquesne, S.; Le Bras, M.; Bourbigot, S.; Delobel, R.; Camino, G.; Eling, B.; Lindsay, C.; Roels, T.; Vezin, H. Mechanism of fire retardancy of polyurethanes using ammonium polyphosphate. *J. Appl. Polym. Sci.* **2001**, *82*, 3262–3274.
47. Schartel, B.; Weiß, A.; Mohr, F.; Kleemeier, M.; Hartwig, A.; Braun, U. Flame retarded epoxy resins by adding layered silicate in combination with the conventional protection-layer-building flame retardants melamine borate and ammonium polyphosphate. *J. Appl. Polym. Sci.* **2010**, *118*, 1134–1143.
48. Bugajny, M.; Bras, M.L.; Bourbigot, S. New approach to the dynamic properties of an intumescent material. *Fire Mater.* **1999**, *23*, 49–51.
49. Jimenez, M.; Duquesne, S.; Bourbigot, S. High-throughput fire testing for intumescent coatings. *Ind. Eng. Chem. Res.* **2006**, *45*, 7475–7481.
50. Duquesne, S.; Magnet, S.; Jama, C.; Delobel, R. Intumescent paints: Fire protective coatings for metallic substrates. *Surf. Coat. Technol.* **2004**, *180–181*, 302–307.
51. Bartholmai, M.; Schriever, R.; Schartel, B. Influence of external heat flux and coating thickness on the thermal insulation properties of two different intumescent coatings using cone calorimeter and numerical analysis. *Fire Mater.* **2003**, *27*, 151–162.
52. Bartholmai, M.; Schartel, B. Assessing the performance of intumescent coatings using bench-scaled cone calorimeter and finite difference simulations. *Fire Mater.* **2007**, *31*, 187–205.

53. Hornsby, P.R.; Mthupha, A. Rheological characterization of polypropylene filled with magnesium hydroxide. *J. Mater. Sci.* **1994**, *29*, 5293–5301.
54. Kim, S. Flame retardancy and smoke suppression of magnesium hydroxide filled polyethylene. *J. Polym. Sci. B Polym. Phys.* **2003**, *41*, 936–944.
55. Haurie, L.; Fernández, A.I.; Velasco, J.I.; Chimenos, J.M.; Lopez Cuesta, J.M.; Espiell, F. Thermal stability and flame retardancy of LDPE/EVA blends filled with synthetic hydromagnesite/aluminium hydroxide/montmorillonite and magnesium hydroxide/aluminium hydroxide/montmorillonite mixtures. *Polym. Degrad. Stabil.* **2007**, *92*, 1082–1087.
56. Braun, U.; Schartel, B. Flame retardant mechanisms of red phosphorus and magnesium hydroxide in high impact polystyrene. *Macromol. Chem. Phys.* **2004**, *205*, 2185–2196.
57. Beyer, G. Flame retardant properties of eva-nanocomposites and improvements by combination of nanofillers with aluminium trihydrate. *Fire Mater.* **2001**, *25*, 193–197.
58. Tsuchiya, Y.; Sumi, K. Thermal decomposition products of polypropylene. *J. Polym. Sci.* **1969**, *7*, 1599–1607.
59. Kiran, E.; Gillham, J.K. Pyrolysis-molecular weight chromatography: A new on-line system for analysis of polymers. II. Thermal decomposition of polyolefins: Polyethylene, polypropylene, polyisobutylene. *J. Appl. Polym. Sci.* **1976**, *20*, 2045–2068.
60. Hornsby, P.R. The application of magnesium hydroxide as a fire retardant and smoke-suppressing additive for polymers. *Fire Mater.* **1994**, *18*, 269–276.
61. Rothon, R.N.; Hornsby, P.R. Flame retardant effects of magnesium hydroxide. *Polym. Degrad. Stab.* **1996**, *54*, 383–385.
62. Wu, G.M.; Schartel, B.; Kleemeier, M.; Hartwig, A. Flammability of layered silicate epoxy nanocomposites combined with low-melting inorganic ceepree glass. *Polym. Eng. Sci.* **2012**, *52*, 507–517.